

Behavior of charmonium systems after deconfinement

Saumen Datta* and Frithjof Karsch†

Fakultät für Physik, Universität Bielefeld, D-33615 Bielefeld, Germany

Peter Petreczky‡

Physics Department, Brookhaven National Laboratory, Upton, New York 11973, USA

Ines Wetzorke§

NIC/DESY Zeuthen, Platanenallee 6, D-15738 Zeuthen, Germany

(Received 18 January 2004; published 20 May 2004)

We present a study of charmonia in hot gluonic plasma, for temperatures up to three times the deconfinement transition temperature T_c . $q\bar{q}$ systems with quark masses close to the charm mass and different spin-parity quantum numbers were studied on very fine isotropic lattices. The analysis of temporal correlators, and spectral functions constructed from them, shows that the J/ψ and η_c survive up to quite high temperatures, with little observable change up to $1.5T_c$, and then gradually weaken and disappear by $3T_c$. For the scalar and axial vector channels, serious modifications are induced by the hot medium already close to T_c , possibly dissociating the mesons by $1.1T_c$.

DOI: 10.1103/PhysRevD.69.094507

PACS number(s): 11.15.Ha, 12.38.Gc, 12.38.Mh, 25.75.Nq

I. INTRODUCTION

The behavior of strongly interacting matter in a hot and dense environment has been a subject of considerable theoretical and experimental research. At very high temperatures and densities, hadronic matter is expected to undergo a phase transition (or crossover) to a deconfined plasma state. Dedicated heavy-ion collision experiments are aiming to create this state, the study of which will enrich our understanding of strong interactions and which is also directly relevant for the early Universe. The suppression of the J/ψ peak in the dilepton spectrum is one of the most important signals of this phase transition. Unlike light quarks, charmonia may survive as bound states even in a deconfined medium, due to Coulomb attraction between the quarks. However, based on non-relativistic arguments, Matsui and Satz predicted that already at temperatures close to T_c , binding between quarks is reduced enough to dissolve J/ψ , and they proposed its suppression as a signal of the deconfinement transition [1]. Several later studies, based on potential model calculations, predicted a pattern of dissolution, with the higher excitations dissolving earlier, and J/ψ dissolving at a temperature $\approx 1.1T_c$ [2,3].

Since the validity of such potential model calculations at high temperatures is not *a priori* clear, a more reliable way of studying properties of charmonia in a hot medium is clearly desirable. One possibility is to directly analyze the thermal Green functions of the corresponding states. For a long time it has been thought that numerical study of lattice is not a practical tool for calculations of dynamic properties of QCD at finite temperature. However, it was shown

recently that meson spectral functions, which are directly related to the real-time correlators, can be extracted from temporal correlators calculated on the lattice using the maximum entropy method (MEM) [4,5]. Some earlier investigations of meson spectral functions (without the use of MEM) were presented in [6]. The method has been successfully applied at zero temperature [4,5,7,8]. Additional difficulties are present at finite temperature because of the finite physical extent of the Euclidean time direction. However, the methods of Ref. [5] were applied successfully to gain qualitative information about the medium modification of mesonic states with temperature [9–11]. Such studies have provided useful quantitative information about dilepton rates [10], and quite unexpected nontrivial structure of the low-energy spectral function for the $\bar{s}s$ mesonic states [11].

First applications of such methods to charmonium systems also produced interesting and unexpected results [12,13]. The ground-state charmonia, η_c and J/ψ , were found to survive well after the deconfinement transition, at least up to temperatures of $1.5T_c$ [12], and no significant modifications of their masses were found on crossing the transition temperature [13]. Both these features are in sharp contrast to the existing potential model studies. The $1P$ states χ_c^0 and χ_c^1 , on the other hand, were found to undergo serious temperature modifications, possibly dissolution, already very close to T_c [12]. Later studies confirmed these results, and also found evidence of the disappearance of the $1S$ states from the spectral function at higher temperatures [14,15].

In the present paper, we are going to report a detailed study of finite-temperature charmonium correlators and spectral functions in quenched QCD using very fine isotropic lattices, expanding on preliminary results published in [12,15]. The plan of the paper is as follows. In the next section, we give a short discussion of the definition of the spectral function and its properties. Section III gives details

*Electronic address: saumen@physik.uni-bielefeld.de

†Electronic address: karsch@physik.uni-bielefeld.de

‡Electronic address: petreczk@quark.phy.bnl.gov

§Electronic address: Ines.Wetzorke@desy.de

of our lattices and simulation parameters. In Sec. IV we explain our analysis methods, giving a short outline of the maximum entropy method. We then present the results below the deconfining transition, which allows us to explain some features of our analysis that are used later. Section V is the central part of the paper, where we present our results for the charmonium correlators and spectral functions above T_c . Study of the systematics is a crucial part of the MEM analysis, at least at the current stage of the finite-temperature mesonic spectral function studies. Therefore, a detailed discussion of the dependence of the results of Sec. V on different systematics follows in Sec. VI. In the next section, we discuss the spatial correlators and screening masses of charmonia, which show some interesting thermal effects and lead us to in-medium modifications of the dispersion relations for the J/ψ . Finally, Sec. VIII contains a summary of our results, along with their phenomenological implications. We also briefly discuss here some points regarding the potential model studies. Readers who are interested in heavy-ion phenomenology but not particularly interested in the details of our analysis may concentrate on Secs. V and VIII.

II. SPECTRAL FUNCTION AND STATES AT FINITE TEMPERATURE

Most dynamic properties of thermal systems are incorporated in the spectral function. The spectral function $\sigma_H(p_0, \vec{p})$ for a given mesonic channel H in a system at temperature T can be defined through the Fourier transform of the real-time two-point functions $D^>$ and $D^<$, or equivalently, as the imaginary part of the Fourier transformed retarded correlation function [16],

$$\sigma_H(p_0, \vec{p}) = \frac{1}{2\pi} [D_H^>(p_0, \vec{p}) - D^>(p_0, \vec{p})],$$

$$D_H^{>(<)}(p_0, \vec{p}) = \int \frac{d^4x}{(2\pi)^4} e^{ip \cdot x} D_H^{>(<)}(x_0, \vec{x}), \quad (1)$$

$$D_H^>(x_0, \vec{x}) = \langle J_H(x_0, \vec{x}) J_H(0, \vec{0}) \rangle,$$

$$D_H^<(x_0, \vec{x}) = \langle J_H(0, \vec{0}) J_H(x_0, \vec{x}) \rangle. \quad (2)$$

The correlators $D_H^{>(<)}(x_0, \vec{x})$ satisfy the well-known Kubo-Martin-Schwinger (KMS) condition [16]

$$D_H^>(x_0, \vec{x}) = D^<(x_0 + i/T, \vec{x}). \quad (3)$$

Inserting a complete set of states in Eq. (1) and using Eq. (3), one gets the expansion

$$\begin{aligned} \sigma_H(p_0, \vec{p}) &= \frac{(2\pi)^2}{Z} \sum_{m,n} (e^{-E_n/T} \pm e^{-E_m/T}) \\ &\times |\langle n | J_H(0) | m \rangle|^2 \\ &\times \delta^4(p_\mu - k_\mu^n + k_\mu^m), \end{aligned} \quad (4)$$

where Z is the partition function, and $k^{n(m)}$ refers to the four-momenta of the state $|n(m)\rangle$.

A stable mesonic state contributes a δ -function-like peak to the spectral function,

$$\sigma_H(p_0, \vec{p}) = |\langle 0 | J_H | H \rangle|^2 \epsilon(p_0) \delta(p^2 - m_H^2), \quad (5)$$

where m_H is the mass of the state. For an unstable particle one gets a smoother peak, with the peak width being related to the decay width. For sufficiently small decay width, a Breit-Wigner form is commonly used. As one increases the temperature, due to collision broadening the contribution of the states in the spectral function change, and at sufficiently high temperatures, the contribution from a state in the spectral function may be sufficiently weakened and broadened that it is not very meaningful to speak of it as a resonance anymore. Such a change of contributions of resonance states and eventual ‘‘disappearance of resonances’’ in the thermal spectral function has been studied analytically, for example in the Nambu-Jona-Lasinio model in Ref. [17]. Finally, at very high temperatures one would expect the spectral function to consist only of a smooth continuum starting at twice the charm quark mass. The spectral function as defined in Eq. (4) can be directly accessed by high-energy heavy-ion experiments. For example, the spectral function for the vector current is directly related to the differential thermal cross section for the production of dilepton pairs [18]:

$$\left. \frac{dW}{dp_0 d^3p} \right|_{\vec{p}=0} = \frac{5\alpha^2}{27\pi^2} \frac{1}{p_0^2 (e^{p_0/T} - 1)} \sigma_V(p_0, \vec{p}). \quad (6)$$

The presence or absence of a bound state in the spectral function will manifest itself in the peak structure of the differential dilepton rate.

In finite-temperature lattice calculations, one calculates Euclidean time propagators, usually projected to a given spatial momentum:

$$G_H(\tau, \vec{p}) = \int d^3x e^{i\vec{p} \cdot \vec{x}} \langle T_\tau J_H(\tau, \vec{x}) J_H(0, \vec{0}) \rangle_T, \quad (7)$$

where $\langle \rangle_T$ means thermal average and T_τ means ordering in Euclidean time τ . This quantity is the analytic continuation of $D^>(x_0, \vec{p})$,

$$G_H(\tau, \vec{p}) = D^>(-i\tau, \vec{p}). \quad (8)$$

Using this equation and the KMS condition, one can easily show that $G_H(\tau, \vec{p})$ is related to the spectral function, Eq. (1), by an integral equation,

$$G_H(\tau, \vec{p}) = \int_0^\infty d\omega \sigma_H(\omega, \vec{p}) K(\omega, \tau), \quad (9)$$

$$K(\omega, \tau) = \frac{\cosh[\omega(\tau - 1/2T)]}{\sinh(\omega/2T)}. \quad (10)$$

Inverting Eq. (9), one can extract spectral functions and properties of hadrons from correlators calculated in lattice QCD. In what follows, we use Eq. (9) to extract the behavior of degenerate heavy meson systems in a thermal medium from finite-temperature mesonic correlators. Equation (10) is

TABLE I. Lattice parameters. The lattice spacing is obtained from the string tension.

β	a^{-1} (GeV)	c_{sw}	κ_c	Size	T/T_c	No. conf.
6.499	4.04	1.494176	0.13558	$48^3 \times 24$	0.62	50
				$48^3 \times 16$	0.93	50
				$48^3 \times 12$	1.24	50
				$48^3 \times 10$	1.49	45
6.64	4.86	1.457898	0.13495	$48^3 \times 24$	0.75	100
				$48^3 \times 16$	1.12	50
				$48^3 \times 12$	1.5	60
7.192	9.72	1.35500	0.13437	$40^3 \times 40$	0.9	85
				$64^3 \times 24$	1.5	80
				$48^3 \times 16$	2.25	100
				$48^3 \times 12$	3.0	90

valid only in the continuum. It is not clear in general whether $G(\tau, \vec{p})$ calculated on the lattice will satisfy the same spectral representation, but it was shown in Ref. [19] that this is the case for the free theory.

III. DETAILS OF THE LATTICE AND SIMULATION PARAMETERS

In this work, we restrict ourselves to the quenched approximation and use pure gauge lattices generated using the isotropic Wilson action. In order to have enough points in the temporal direction at high temperatures, we need very fine lattices. We use lattices at three different lattice spacings in the range 0.02–0.05 fm. At the higher temperatures only the finer lattices are used, while at the lower temperatures, comparison between results from our finer and coarser lattices gives an idea of the effect of the limited number of data points in our analysis. The lattices were generated using the heat-bath and overrelaxation algorithm, with each sweep consisting of one heat-bath step followed by four overrelaxation steps. The configurations were separated by 200–800 such sweeps, the separation in each case being five to eight times the autocorrelation time of the Polyakov loop. The exact details of the lattices was given in Table I. A subset of these lattices was used for the light meson studies of Ref. [10].

For the valence quarks, we use the clover-improved [20] Wilson action, taking the clover coefficients from the non-perturbative estimates of the ALPHA Collaboration [21]. The clover coefficients used, and the critical coupling κ_c at each β , are shown in Table I. For our coarsest lattice, we use three κ values that bracket the charm, giving a pseudoscalar mass in the range 1.7–4 GeV. This allows us to study the mass dependence of the properties that we are considering. At the finer lattices, we use one κ value close to the charm mass.

In order to study the lowest states in each of the four channels, we take operators with four different spin structures. The operators we study are listed below, along with the names and spectroscopic representations of the lowest states for each channel:

$$J_H = \begin{array}{lll} \bar{c}c & {}^3P_0 & \chi_c^0 \\ \bar{c}\gamma_5c & {}^1S_0 & \eta_c \\ \bar{c}\gamma_\mu c & {}^3S_1 & J/\psi \\ \bar{c}\gamma_\mu\gamma_5c & {}^3P_1 & \chi_c^1. \end{array} \quad (11)$$

For zero-temperature spectrum studies, smeared operators are usually used to increase the overlap with the ground state, so one can study the ground-state properties already from correlators at small distance. However, when one wants to study other properties of a channel, for example meson decay constants, one has to be careful about using smeared operators. Here since we will be interested mostly in the existence versus dissolution of the states, it is tricky to use smeared operators. Smearing mimics bound states even when there are none [9], and it is also difficult to extract phenomenological quantities, such as the dilepton rate in Eq. (6), if one works with smeared operators. Therefore, we use point-to-point correlators in this study. When one knows that there are bound states, it may be better to use the smeared operators to calculate the mass of the states.

The use of the nonperturbative clover action removes $\mathcal{O}(a)$ discretization errors. However, in the case of heavy quarks, discretization errors of order $\mathcal{O}(am)$ can be large. The errors in using the clover quarks due to finite mass of the quarks have been discussed in detail in Ref. [22]. The main sources of $\mathcal{O}(ma)$ errors are in the difference between the pole mass and the kinetic mass, and in the renormalization constant used to connect the lattice operators to continuum ones. For finite ma , the pole mass that controls the fall-off of the correlator differs by $\mathcal{O}(ma)$ terms from the physically important kinetic mass that controls the dispersion relation. This can already be seen from the free quark dispersion relations [22],

$$\begin{aligned} am_0 &= \frac{1}{2\kappa} - \frac{1}{2\kappa_c}, \\ am_{\text{pole}} &= \ln(1 + am_0), \\ am_{\text{kinetic}} &= \frac{am_0(1 + am_0)(2 + am_0)}{2 + 4am_0 + m_0^2}, \end{aligned} \quad (12)$$

where m_0 is the standard definition of the bare mass, m_{pole} governs the fall-off of the free quark correlator, and m_{kinetic} is the term governing the quadratic momentum dependence in the dispersion relation, and therefore controlling much of the spectrum and other interesting physics in heavy quark systems. A large mismatch between m_{pole} and m_{kinetic} indicates that the quark is too heavy to be treated relativistically. Our lattices are fine enough that in most cases the error due to the finite mass of the charm quark is small enough. The hopping parameters we have used for our different lattices are listed in Table II. We also list there the tree-level pole and kinetic masses, using Eq. (12). The tree-level mismatch between m_{pole} and m_{kinetic} is $< 5\%$ for all the sets, except the heaviest quark for set I. To see whether the error is also small for the interacting theory, we also looked at the pole and kinetic

TABLE II. Hopping parameters used and the pole and kinetic masses for different sets.

β	κ	am_{pole}	am_{kinetic}	am_0	Tag
6.499	0.1325	0.0889	0.0893	0.0860	I A
	0.1300	0.1584	0.1608	0.1583	I B
	0.1234	0.3328	0.3531	0.3640	I C
6.64	0.1290	0.1800	0.1835	0.1821	II
7.192	0.13114	0.0940	0.0945	0.0916	III

masses of the mesons, where the pole mass is obtained from the zero-momentum correlator and the kinetic mass is obtained from the dispersion relation

$$E^2 = M_{\text{pole}}^2 + \frac{M_{\text{pole}}}{M_{\text{kin}}} p^2. \quad (13)$$

While M_{kin} is quite noisy, we found that there is hardly any significant deviation from the relativistic dispersion relation for the quark masses used by us, except possibly for set IC [23]. We therefore use a relativistic treatment for our quarks in what follows, and set the masses of the mesons from the pole masses.

The lattice operators are connected to the continuum operators as

$$J_H^{\text{cont}} = 2\kappa Z_H(a, m, \mu = 1/a) J_H^{\text{lat}} a^{-3}. \quad (14)$$

The renormalization factors $Z_H(a, m, \mu = 1/a)$ are estimated using one-loop tadpole improved perturbation theory,

$$Z_H(a, m, \mu = 1/a) = u_0(a) [1 + \alpha_V(1/a) \tilde{z}_H] [1 + b_H(a) m a], \quad (15)$$

$$b_H(a) = [1 + \alpha_V(1/a) \tilde{b}_H] / u_0. \quad (16)$$

Here $\alpha_V(1/a)$ is the running coupling calculated from the heavy quark potential at scale $\mu = 1/a$ [24]. The one-loop coefficients \tilde{z}_H and \tilde{b}_H were calculated in Refs. [25] and [26], respectively. For the scalar and pseudoscalar channels, \tilde{z}_H was evaluated at scale $\mu = 1/a$. We evaluate u_0 from the measured plaquette,

$$u_0 = \langle \frac{1}{3} \text{Tr} U_{\text{plaq}} \rangle^{1/4}.$$

The resulting renormalization factors are shown in Table III.

TABLE III. Renormalization factors of local operators for different sets.

β	κ	Z_{PS}	Z_{SC}	Z_{VC}	Z_{AX}
6.499	0.1325	0.782	0.839	0.900	0.926
	0.1300	0.847	0.913	0.975	1.003
	0.1234	1.032	1.124	1.188	1.221
6.64	0.1290	0.881	0.948	1.007	1.034
7.192	0.13114	0.839	0.886	0.936	0.957

TABLE IV. Masses (in GeV) of the different charmonium states obtained from one exponential fits of spatial correlators below T_c .

Set	Mass (in GeV)			
	η_c	J/ψ	χ_{c0}	χ_{c1}
I A	1.673(8)	1.806(8)	2.151(27)	2.299(44)
I B	2.440(5)	2.517(10)	2.874(30)	3.006(31)
I C	4.151(4)	4.191(6)	4.600(44)	4.670(48)
II	3.071(6)	3.141(12)	3.526(53)	3.622(117)
III	3.744(14)	3.803(10)	4.442(86)	4.666(174)

We close this section with a discussion of the zero-temperature masses of the charmonia corresponding to the κ values given in Table II. For our coarsest lattices, we use three κ values that bracket the charm quark. For the other lattices, we use one κ value each. Since we have not performed calculations on symmetric (zero-temperature) lattices, our estimates of the zero-temperature masses are based on exponential fits to spatial correlators. In fact, if one considers the spatial correlators on lattices below deconfinement, the finite-temperature lattices can be considered as small (in one of the directions) zero-temperature lattices. For the lattices below T_c used in this study (see Table I), the small extent is about 1 fm for the two coarser lattices (sets I and II) and about 0.8 fm for the finest lattice (set III). The effect of finite volume on the masses of charmonia was studied in detail in [27] and it was found that even for lattices of size 0.75 fm there are no sizeable finite-size effects. Furthermore, even for the much larger light mesons, spatial correlators calculated on lattices at $0.9T_c$ have been seen to give good estimates of zero-temperature masses [28]. The masses we get from exponential fits are given in Table IV.

For set II, which is very close to the physical value of the charm quark mass, we get 70 ± 12 MeV for the hyperfine splitting, consistent with the analysis of Ref. [27]. The mass splitting between P and S states is also consistent with the findings of [27]. For our finest lattices, the splitting between P and S states is largely overestimated. This could be due to the limited (~ 0.82 fm) extent of the lattice.

IV. MESON CORRELATORS AND SPECTRAL FUNCTIONS FOR $T < T_c$

We begin our discussion of spectral functions and temperature effects on meson properties with an analysis of the meson correlators below T_c . We look at the temporal correlators, Eq. (7), for the four channels in Eq. (11) and for the lattices with $T < T_c$ as specified in Table I. For the lattices at $\beta = 6.64$ and 7.192 , we have one set each below T_c , the spatial correlators from which were used in the previous section for setting the parameters. Here we use the temporal correlators and investigate the spectral function at temperatures $T \leq T_c$. On our coarsest set at $\beta = 6.499$, we have lattices corresponding to two different temperatures below T_c . This allows us to check for any change in meson properties as one approaches T_c from below. For most of this study we use zero-momentum projected correlators only, and refer to them as $G(\tau)$, and the corresponding spectral function as

$\sigma(\omega)$ (we also suppress the subscript H from now on).

The operators corresponding to the different channels have been listed in Eq. (11). For the vector channel, we take the trace over all four directions, $\sum_{\mu=0}^3 G_{\mu\mu}^{\text{VC}}(\tau)$. Due to current conservation, the time component, $G_{00}^{\text{VC}}(\tau)$, is a constant, and therefore contributes only a δ function at $\omega=0$ to the spectral function. In the free quark case, this δ function cancels a similar contribution from the space-averaged correlator [31]. In the axial vector channel, we sum over the three spatial directions, $\sum_{i=1}^3 G_{ii}^{\text{AV}}(\tau)$.

At least in principle, one can obtain all the information about the spectrum in a given channel by inverting Eq. (9) to calculate $\sigma(\omega)$. Since our lattices have only $O(10)$ independent data points in the temporal direction, however, extracting $\sigma(\omega)$ from lattice data for $G(\tau)$ is a highly nontrivial problem. Considerable progress towards the solution of this problem has been made in the last couple of years by using the Bayesian methods [5]. In the next subsection, we explain the rudiments of the maximum entropy method (MEM), as employed in our analysis; in the rest of this section, we use this method to extract the spectral function, and discuss the results.

A. Analysis: MEM methods

Bayesian techniques for extracting information from inadequate data depend on providing prior information to the analysis in some form [29]. In the MEM of data analysis, the prior information is usually introduced in the form of an ‘‘entropy term’’ by using the positivity of the spectral function [$\sigma(\omega>0)\geq 0$] to give it a probability interpretation [29]. Quite general principles lead to the Shannon entropy

$$S = \int_0^\infty d\omega \{ \sigma(\omega) - m(\omega) - \sigma(\omega) \log[\sigma(\omega)/m(\omega)] \} \quad (17)$$

(see Refs. [5,29] for justifications for the form of the entropy term). The entropy depends on an arbitrary function $m(\omega)$, which is called the default model. This function can be considered as a part of our prior information. The central problem becomes then to find the $\sigma(\omega)$ that maximizes the ‘‘free energy’’

$$F = L - \alpha S \quad (18)$$

or equivalently the conditional probability $P[\sigma|DH]$ of having the spectral function σ given some data D and the prior knowledge H [29]. Here L is the likelihood function for the data D , i.e., $L = \chi^2/2$, and α is a real and positive parameter.

At zero temperatures, MEM has been successfully applied in spectrum calculations [4,5,7,8]. At finite temperatures, where one is limited further by the small physical extent of the temporal direction, precise quantitative information is more difficult to obtain. Still, useful qualitative information has been obtained about the shape of the spectrum and the thermal dilepton rate [9–11].

We follow here Bryan’s algorithm [30] for inverting Eq. (9). This method uses a singular value decomposition of the kernel, to find the relevant, nonsingular directions in the in-

version process, which are less than the number of data points. Then the search for solutions is restricted to this space, which is now a well-defined problem. Also, in this algorithm one avoids any explicit dependence on the external parameter α in Eq. (18) by integrating over α with a conditional probability (see [5,30] for details).

To reconstruct the spectral function, the default model $m(\omega)$ needs to be specified. Since we want to explore the modification of the ground-state peaks in the spectral function, it is natural to choose the default model to describe only the high-energy part of the spectral function. Due to asymptotic freedom, the spectral function at very high energies is expected to approach the case of two free quarks. For two free quarks in a mesonic channel H , the spectral function in the continuum is given by [31]

$$\sigma_H(\omega) = \frac{3}{8\pi^2} \omega^2 \Theta(\omega^2 - 4m^2) \tanh(\omega/4T) \sqrt{1 - 4m^2/\omega^2} \times \left(a_H + \frac{4m^2}{\omega^2} b_H \right) \quad (19)$$

$$\approx \frac{3}{8\pi^2} a_H \omega^2 \quad \text{for } \omega \rightarrow \infty. \quad (20)$$

For the scalar, pseudoscalar, vector, and axial vector channels, the constants a_H are 1, 1, 2, and 2, respectively [31]. On the lattice, the spectral functions for the different channels have been calculated recently for the free theory [19]. They show a considerably different high-energy structure from Eq. (20). Interaction introduces additional modification of the large ω behavior of the spectral function [8]. At low temperatures, where the temporal extent is relatively large and the dependence on the default model is less important, we use $m(\omega) = m_0 \omega^2$ for the default model, with $m_0 = 3/(8\pi^2)$ for scalar and pseudoscalar channels and $m_0 = 3/(4\pi^2)$ for vector and axial vector channels. The lattice introduces an ultraviolet energy cutoff

$$\omega_{\text{max}} = \frac{2}{a} \ln(7 + am_0) \approx 4a^{-1}$$

for our masses. This is the frequency cutoff we use in our analysis. Above T_c the use of a more refined form of the default model, with more accurate information about the high-energy structure of the interacting theory, becomes necessary, which we discuss in the next subsection.

Use of the full covariance matrix is desirable in the MEM analysis. However, it has been shown that with limited statistics sometimes the small eigenvalues of the covariance matrix can be too noisy and it may be better to use some smoothing of the smaller eigenvalues [33]. In our analysis, we use the full covariance matrix in most cases; but sometimes the use of the full matrix gives rise to an unphysical peak at $\omega \sim 0$. In such cases, we use the minimum smoothing that can get rid of this peak, if it is possible with a small amount of smoothing.

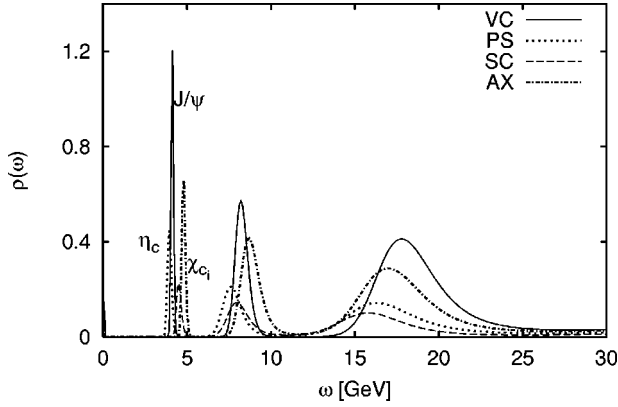


FIG. 1. Spectral functions at $0.9T_c$ for the different channels, for set III.

For the spectral density extracted from noisy data with MEM, one can assign error bars to the spectral density integrated over small regions of frequency (see Ref. [29]): one defines an “integrated spectral density,”

$$H(\omega, \Delta) = \int_{\omega-\Delta}^{\omega+\Delta} d\omega \sigma(\omega)$$

and then the covariance of this quantity is calculated as

$$\langle \delta H^2 \rangle = \int d\omega \int d\omega' \sigma(\omega) \sigma(\omega'). \quad (21)$$

Since we are concerned with the peak structures in the spectral function, in the following sections we show the error bars on a region integrated over the peak width of each peak, to show the statistical significance of the peaks.

B. Discussion of the spectral functions

As mentioned in the previous section, the reliability of the spectral function reconstructed from the temporal correlators using MEM depends on the number of data points. We start the reconstruction of spectral functions below T_c on our finest lattice: set III. Besides allowing us to have the maximum resolution, fine-graining of the lattice also has the advantage that the lattice artifacts are shifted further away from the ground-state peaks, allowing an accurate extraction of the ground-state peaks of interest.

Figure 1 shows the spectral functions at $0.9T_c$, reconstructed from the correlators for this set in the different channels. In order to remove the uninteresting ω^2 rise in the spectral function, here and in everywhere else we plot the “reduced spectral function”

$$\rho(\omega) = \sigma(\omega)/\omega^2. \quad (22)$$

At $T=0.9T_c$, the physical distance available for the analysis of the temporal correlators is about 0.82 fm, and we have 40 data points. This allows us to have a good resolution of the ground-state spectral function. We also found that omitting the data point at smallest τ enhances the peak structure for this set. In each channel we find a three-peak structure, with the ground-state peak replicating quite well the

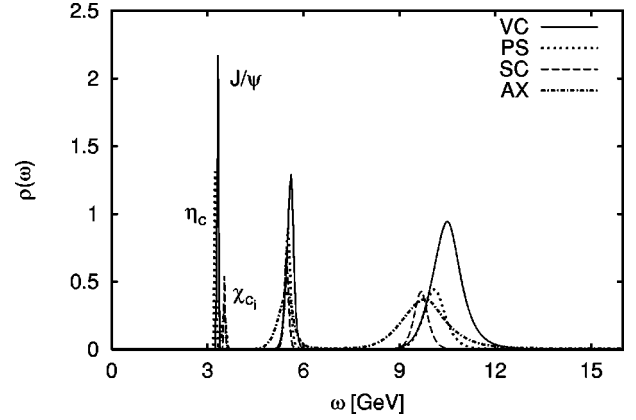


FIG. 2. Spectral functions at $0.75T_c$ for the different channels, for set II.

properties of the zero-temperature ground state in Table IV. We also find that for energies $\omega \sim 2/a$, where the doubler states are expected to contribute, the structure of the spectral function is considerably different from the free spectral function. Similar peaklike structures have been seen in [8]. As we explain below, we expect the additional peak seen at $\omega \sim 1/a$ is also a lattice artifact.

A comparison with the spectral structure obtained from set II helps in clarifying the nature of the second peak in Fig. 1. The spectral functions in different channels for this set are presented in Fig. 2. For this figure we use again the free lattice spectral function as the default model. The properties of the zero-temperature peak in Table IV are reproduced quite well. The other peaks are seen to shift at approximately the same ratio from Fig. 1 as the inverse lattice spacing. This confirms that also the second peak obtained in Figs. 1 and 2 is dominated by lattice artifacts.

In our coarsest set of lattices, at $\beta=6.499$, we have two temperatures below T_c . This allows us to study the temperature dependence of the mesons below T_c , and will help in introducing certain elements in our analysis, as we will see below.

For the correlators at $0.6T_c$, the results are shown for set IB in Fig. 3. We get a three-peak structure for the different channels, similar to the one shown in the previous figures. The ground state can be resolved quite reliably, and the strength and position of the ground state for the different quark masses agree with the ground-state measurements obtained in the previous section.

Figure 4 compares the spectral functions for the vector channel at 0.6 and $0.9T_c$, obtained with the free spectral function as the default model. The high ω part of the spectral function at $0.9T_c$ is seen to be considerably different from that at $0.6T_c$. Also, while $\rho(\omega)$ shows a clear ground-state peak, the peak position is slightly changed from that at $0.6T_c$ and the fall-off of the peak in the high ω side is considerably broader. However, we expect this difference in the spectral function to be an artifact of the limited number of data points and physical distance at this temperature. In fact, Fig. 4 does indicate that at $0.9T_c$, the spectral analysis cannot resolve the three-peak structure, and the ground-state peak is contaminated by the peak at $\omega \sim 1/a$. One way to improve the

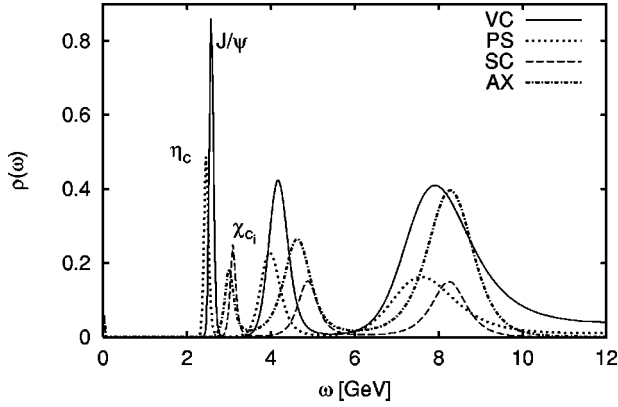


FIG. 3. Spectral functions for different channels at $0.6T_c$ for set IB.

reconstruction of the ground state when the physical distance is small is to provide more accurate information for the high-energy part in the default model. Since the physical distance covered is small, the high-energy part is still important in the correlator and it is only when we provide suitable information about the high-energy part that it is possible to extract the information about the ground state accurately. From the analysis of the spectral function at the lowest temperatures, we see that the high-energy part of the spectral function consists of two broad peaks. This is a general feature of the spectral functions which does not depend on the default model $m(\omega)$, as we will see in Sec. VI. So we use a default model where the high-energy part of the spectral function is taken from the spectral function constructed at $0.6T_c$, and in the low-energy part we use the model

$$m(\omega) = m_1 \omega^2$$

with m_1 chosen such that the default model is continuous [15]. The spectral function constructed at $0.9T_c$ using this default model is also shown in Fig. 4, where for comparison we also show the spectral function at $0.6T_c$ using the same default model. As we can see, at $0.6T_c$ the spectral function

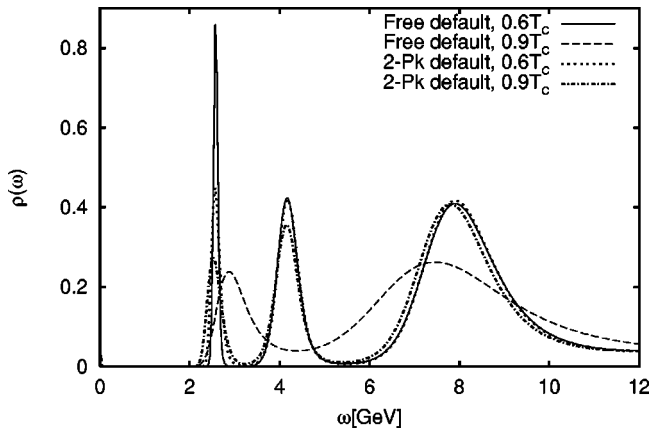


FIG. 4. Spectral functions for the vector channel below T_c , using both the free spectral function and the high energy part of the spectral function from interacting theory as a default model, for set IB.

correctly produces the ground-state peak, in both the position and the strength of the peak. (In our present analysis with limited statistics the width of the peak is not of direct physical relevance. It is possibly an effect of the finite statistics.) Using this default model, now, the ground state at $0.9T_c$ is reconstructed accurately, with the position and strength of the peak similar to that at $0.6T_c$. This also shows the usefulness of using such a default model, and we will use it for reconstructions of the spectral function above T_c in the next section. In essence, what is being done is to realize that the spectral function for very large $\omega \gg T$ is dominated by lattice artifacts, and does not change with temperature. To reconstruct the ground state accurately from correlators at short distances, it is important to use correct information of this high-energy part. Another way to confirm that the spectral function does not show any significant change between $0.9T_c$ and $0.6T_c$ is by comparing the correlators at $0.9T_c$ with the correlators reconstructed from the spectral function at $0.6T_c$ [15]. Since the temperature dependence of the correlators in Eq. (9) comes from both the known temperature dependence of the kernel, $K(\omega, \tau)$, in Eq. (10), and the nontrivial temperature dependence of the spectral function, $\sigma(\omega, \vec{p})$, we can try to focus on the temperature dependence of the spectral function by comparing the correlator with the reconstructed correlator at that temperature,

$$G_{\text{recon}, T^*}(\tau, T) = \int d\omega \sigma(\omega, T^*) K(\omega, \tau, T), \quad (23)$$

where $\sigma(\omega, T^*)$ is the spectral function at another temperature T^* . The comparison of the correlators for the different channels at $0.9T_c$ with the correlators reconstructed from $\sigma(\omega, 0.6T_c)$ for the corresponding channels is shown in Fig. 5. This figure clearly demonstrates that the correlators at $0.9T_c$ are completely described by the spectral function at the lower temperature.

The results from the other quark masses for set I are very similar and show that for the quark mass range explored by us, the properties of the ground-state mesons do not change at least up to a temperature of $0.9T_c$. This is consistent with other earlier quenched studies in the mesonic sector [28] and the gluonic sector [32], which showed that the properties of the mesonic and gluonic states do not change from their vacuum properties until quite close to the deconfinement transition temperature. Of course, this result is not unexpected since one does not expect substantial thermal excitation of the heavy glueballs already at these temperatures. Presumably, such a result may not hold in full QCD, where excitation of pionic states may produce observable effects already away from T_c .

To summarize, in this section we have studied the spectral functions below T_c for heavy degenerate mesons in different channels. The ground-state properties can be suitably reproduced by the MEM analysis of the temporal correlators. We also show that using nontrivial realistic information about the high-energy structure of the spectral function in the interacting theory allows a more accurate reconstruction of the ground state already from short-distance correlators available on a small number of data points. We also propose using the

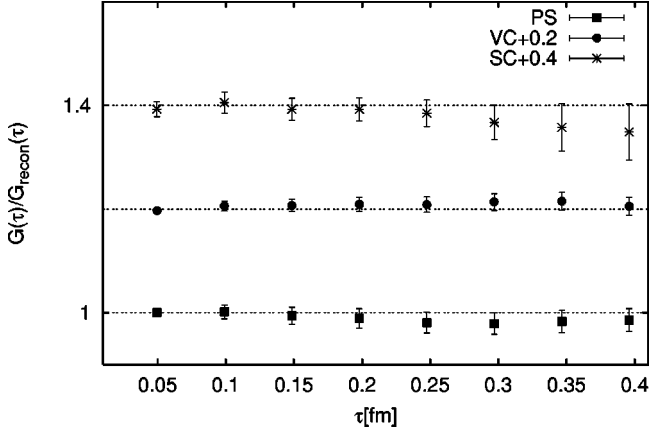


FIG. 5. Ratio of the measured correlators at $0.9T_c$ with the reconstructed correlators at this temperature, using the spectral function at $0.6T_c$ (see text), for different channels and set IB. For visual clarity, the vector and scalar channels have been shifted horizontally.

spectral function constructed at the lowest available temperature to reconstruct the correlator at higher temperatures, as a way of studying the temperature dependence of the spectral function. This often provides a more robust analysis, since the lowest available temperature provides us with the maximum physical distance, allowing for a more reliable extraction of the spectral function. Both these techniques will be particularly relevant in the next section for studying the spectral function above T_c , where small physical distance makes the extraction of the spectral function even more difficult.

V. CORRELATORS AND SPECTRAL FUNCTIONS FOR $T > T_c$

In this section we present our results for meson correlators above T_c . We first present results for set II, so that we can start with results close to T_c , and then go to higher temperatures with set III.

A number of interesting and important statements about system modifications of charmonium spectral functions can be made by inspecting the finite-temperature meson correlators. As was discussed in the previous section, the change in $\sigma(\omega)$ with temperature can be studied already from the correlators, by first taking out the trivial temperature dependence of the kernel $K(\omega, \tau, T)$ according to Eq. (23). We construct $G_{\text{recon}}(\tau, T)$ using $\sigma(\omega, T^*)$ from the spectral functions obtained for this set at $0.75T_c$ (see Fig. 2). The deviations of $G_{\text{recon}}(\tau, T)$ from the correlators directly measured above T_c then indicate system modifications of the spectral function above T_c . This method is more robust as it avoids using MEM at the higher temperatures, where one has less temporal extent and fewer data points.

In Fig. 6(a) we show the results of $G(\tau, T)/G_{\text{recon}}(\tau, T)$ for set II for the pseudoscalar and vector channels (the $1S$ states). For the pseudoscalar channel, the ratio is seen to remain equal to 1 up to $1.5T_c$, indicating no significant system modification of its properties up to this temperature. This is already in sharp contrast to earlier potential model results,

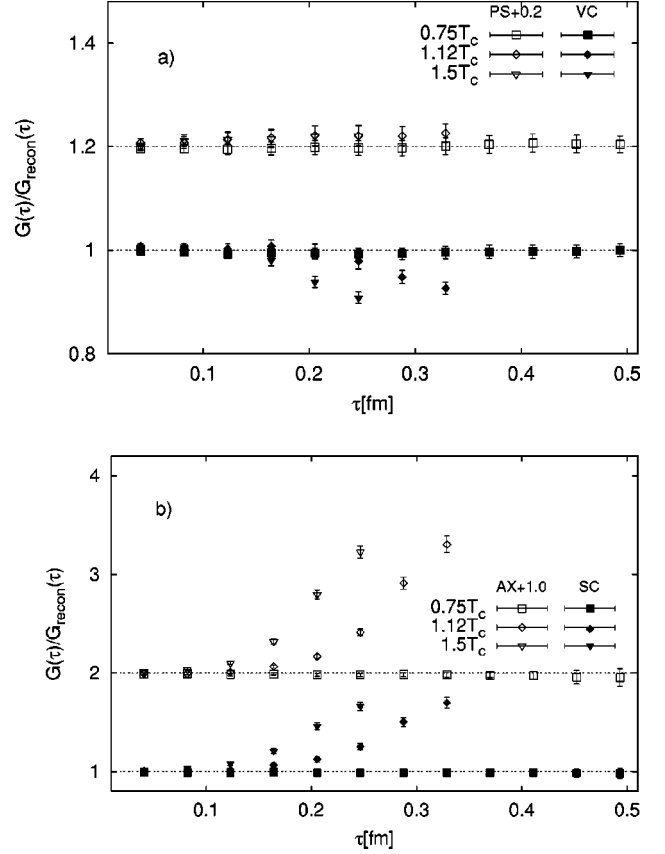


FIG. 6. Ratio of the measured temporal correlators with the correlators reconstructed from the spectral function at $0.75T_c$ for set II. (a) Pseudoscalar (PS) and vector (VC) channels; (b) scalar (SC) and axial vector (AX) channels. For visual clarity, the PS and AX channel results have been shifted vertically.

which predicted a dissolution of η_c at $\approx 1.1T_c$. For the vector channel, one finds that the reconstructed correlator explains the data quite well at small distances. Some significant system modifications, however, are manifested in the correlators at distances > 0.25 fm. At $1.5T_c$, some modifications are already seen at distances ≥ 0.2 fm. Later in this section, we will discuss possible system modifications that can cause such a change.

The correlators for the scalar and axial vector channels (the $1P$ states) are shown in Fig. 6(b). The situation is seen to be quite different here: already at $1.1T_c$, a significant system modification of the mesons is manifested in $G(\tau, T)/G_{\text{recon}}(\tau, T)$ at all distances. The measured correlators are seen to be considerably larger than the reconstructed correlators. Such a behavior can be qualitatively understood if the $1P$ states are dissolved already at these temperatures: at low temperatures, the spectral function for these states is zero below ~ 3.5 GeV. If the state is dissolved above T_c , one would expect the correlator to pick up contributions at significantly smaller $\omega \sim 2m_c$, making it larger.

The comparison with reconstructed correlators can only tell us whether any medium modification can be expected at a given temperature. The ratios of the correlators give a rough idea of the magnitude of such modification. To further explore the nature of the finite-temperature spectral func-

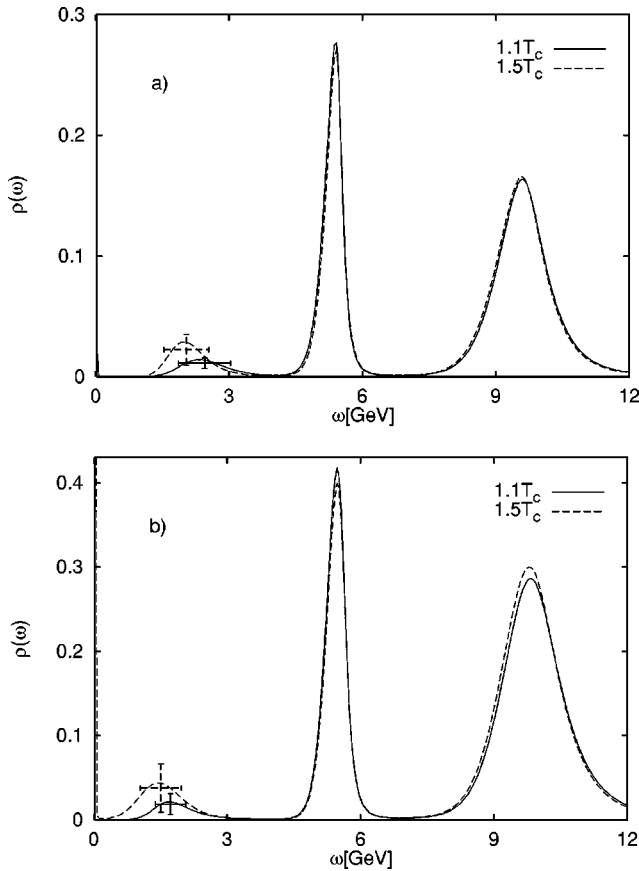


FIG. 7. The spectral function for the (a) scalar and (b) axial vector channels constructed from the temporal correlators, for set II at temperatures between 1.12 and $1.5T_c$. The default model uses the high-energy part of the spectral function in Fig. 2, as explained in the text.

tions, it is necessary to reconstruct the spectral function from the correlators, using MEM. Above T_c , the physical distance available to us is small, and fewer data points are available, making it difficult to reliably extract the spectral function without any prior knowledge. However, as we have discussed in Sec. IV B, by introducing information about the high-energy part of the spectral function into the MEM analysis in the form of an appropriate default model we can overcome this problem. Therefore, in the default model we use the high-energy part of the spectral function at $0.75T_c$, smoothly matched to $m_1\omega^2$ in the low-energy region (see Sec. IV B).

The spectral functions for the scalar and axial vector channels above T_c , reconstructed in this way, are shown in Fig. 7. The significant ground-state peak of Fig. 2 for these channels is not found at these temperatures. A nonzero spectral function is seen at a significantly lower ω , but the peak structure is statistically not significant, and it could be related to a branch cut coming from two on-shell propagating quarks. Such a $\sigma(\omega)$ at low ω can also explain the rise of the correlators seen in Fig. 6(b). Since the quark mass for set II is very close to the physical charm quark (see Table IV), Fig. 7, together with Fig. 6(b), will indicate that the χ_c^0 and the χ_c^1 are seriously modified, possibly dissolved, already at $1.1T_c$.

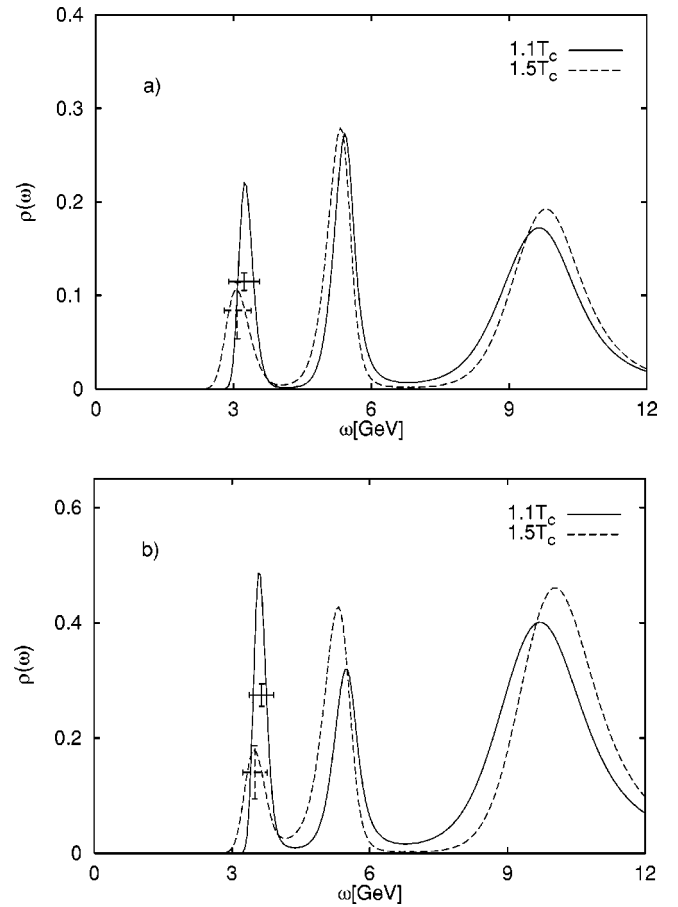


FIG. 8. The spectral function for the (a) pseudoscalar and (b) vector channels constructed from the temporal correlators, for set II at temperatures between 1.12 and $1.5T_c$. The default model uses the high-energy part of the spectral function in Fig. 2, as explained in the text.

The situation is different for the $1S$ states: Fig. 6(a) seems to rule out dissolution or a major modification of these states. The reconstructed spectral functions, shown in Fig. 8, support this: a statistically significant ground-state peak is seen up to $1.5T_c$, showing that the η_c and the J/ψ survive at least up to this temperature. While no major change in mass is indicated, a reduction in peak strength is seen at $1.5T_c$; however, as discussed below and also Sec. VI, Fig. 15, we expect it to be related to the associated systematics.

Having seen that the J/ψ survives until $1.5T_c$, it will be interesting to explore its properties at higher temperatures. Our finest lattices at set III allow us to go up to a temperature of $3T_c$. The finer grid at $1.5T_c$ here also allows one to check the reliability of the results of set II. Figure 9(a) presents $G(\tau, T)/G_{\text{recon}}(\tau, T)$ for different temperatures. $G_{\text{recon}}(\tau, T)$ is constructed using the spectral functions at $0.9T_c$ presented in Fig. 1. Up to $1.5T_c$, the features of Fig. 9(a) are very similar to that of Fig. 6(a). For the pseudoscalar channel, the data are completely explained by the spectral function at $0.9T_c$. Some small, but statistically significant, deviations appear at $2.25T_c$. At $3T_c$, we see significant modification at all distances. For the vector channel, at $1.5T_c$ the data agree with the reconstructed correlator at small distances, but start

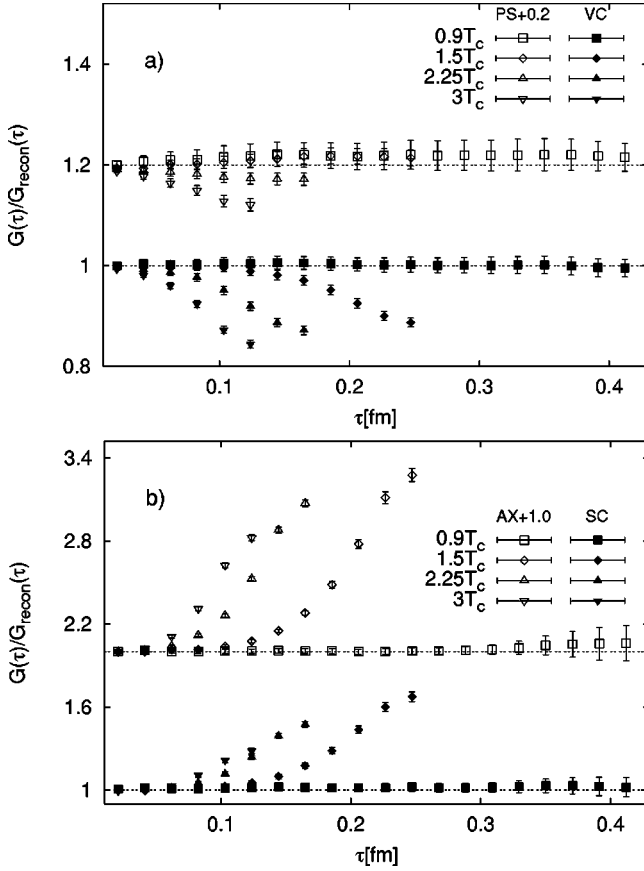


FIG. 9. Ratio of the measured temporal correlators with the correlators reconstructed from the spectral function at $0.9T_c$ for set III. (a) Pseudoscalar (PS) and vector (VC) channels; (b) scalar (SC) and axial vector (AX) channels. For visual clarity, the PS and AX channel results have been shifted vertically.

showing significant modifications at larger distances, $\tau \geq 0.15$ fm. At $2.25T_c$, such modifications appear already at ~ 0.1 fm while at $3T_c$, $G(\tau, T)/G_{\text{recon}}(\tau, T)$ differ significantly from 1 at all distances.

For the scalar and axial vector channels, one sees at $1.5T_c$ a very similar enhancement of the correlator to Fig. 6(b), with $G(\tau, 1.5T_c) \sim 60\%$ larger than $G_{\text{recon}}(\tau, T)$ at ~ 0.25 fm for the scalar and $\sim 120\%$ larger for the axial vector. The pattern of enhancement continues as one goes to higher temperatures.

To extract the spectral function from the temporal correlators above T_c , we use, as input to the default model, the large ω structure shown in Fig. 1. Figure 10(a) shows the spectral functions above T_c obtained with this default model. A strong and statistically significant ground-state peak is obtained at $1.5T_c$. The peak position and peak strength are found to be very similar to those at $0.9T_c$, indicating essentially no significant change for the pseudoscalar up to this temperature. This is completely consistent with the trend seen for $G(\tau, T)/G_{\text{recon}}(\tau, T)$ for the pseudoscalar. At $2.25T_c$, we still see a statistically significant peak, but with a reduced strength, and at $3T_c$ the structure at the peak position is very weak and not statistically significant.

For the vector channel, the temperature dependence of the

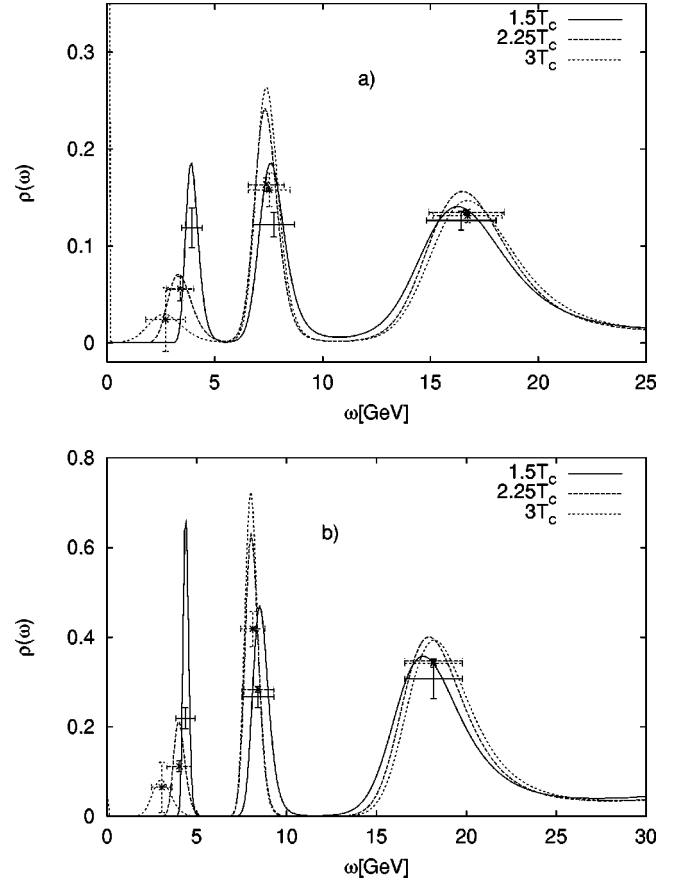


FIG. 10. The spectral function for (a) pseudoscalar and (b) vector channels constructed from the temporal correlators, for set III at temperatures up to $3T_c$. The default model uses the high-energy part of the spectral function in Fig. 1, as explained in the text.

spectral function is very similar. A very strong peak is seen at $1.5T_c$, with no observed reduction in the peak strength from that below T_c . Unlike the pseudoscalar channel, we see here a slight shift of the peak position, but the amount of the shift depends on the systematics and we are unable to make a definite comment on it. At $2.25T_c$, a significant peak is seen with a reduced strength, and at $3T_c$, the structure at the peak position is too broad to be interpreted as a resonance, and is also statistically not significant.

As we will discuss in detail in the next section, the details of the features presented in Fig. 10 and Fig. 8 are not dependent on the systematics incorporated in extracting the spectral function, either from the specifics of the default model or from the small temporal extent and limited number of data points at higher temperatures. The $1S$ state mesons survive with no significant change of strength at least up to $1.5T_c$, and at $2.25T_c$ a significant peak still survives but with a reduced strength, while at $3T_c$ system effects reduce the peak strength enough that one should consider the state to be dissolved. Such a change in the spectral function is also completely consistent with the behavior of $G(\tau, T)/G_{\text{recon}}(\tau, T)$ for the pseudoscalar channel, since a reduced ground-state peak will cause a depletion of $G(\tau)$. For the vector channel, the general picture indicated by Fig. 10(b) is the same. However, we also see here a depletion of $G(\tau)$ at large distances

already at $1.5T_c$, but no reduction of the peak strength in Fig. 10(b), and a small increase in mass. While such an increase in mass at $1.5T_c$ is consistent with the depletion of the correlator, we cannot isolate any physical mass shift from the systematics.

We would like to comment here on similar works on J/ψ in the quark-gluon plasma. Reference [13] uses smeared operators, which allows them to study the properties of the in-medium η_c and J/ψ in more detail, and finds a large Breit-Wigner width ~ 120 MeV and 210 MeV, respectively, at $1.1T_c$. They also find no reduction of the masses of the $1S$ states above T_c . With our point-point correlators, we cannot extract a width reliably; however, any such width will cause an enhancement of the correlator, which we do not see for these states. However, it is possible that such an enhancement is shielded by a corresponding reduction in peak strength. Reference [14] uses point-point correlator, and concludes that the $1S$ states dissociate already at $1.9T_c$. Of course, our quarks for set III are a little heavier than physical charm, and that can cause the mismatch (the mass dependence of the modification pattern is discussed below); however, we think another likely reason could be that due to the use of the free continuum spectral function, Eq. (19), as the default model in Ref. [14] (which does not provide accurate information about the structure of the high-energy part of the spectral function), and the small temporal extent at this temperature, MEM cannot resolve the peak structure correctly.

For our coarsest lattices, set I, we have three quark masses, giving pseudoscalar masses in the range 1.7–4.1 GeV (see Table IV). This allows us to study the mass dependence of the dissolution pattern, i.e., to answer the question whether the “melting temperature” for the quarkonia has a mass dependence.

In Fig. 11 we show the ratio of the pseudoscalar correlators at different temperatures with the correlators reconstructed from spectral function at $0.62T_c$ using Eq. (23). At $0.93T_c$, expectedly, the correlators are explained by the spectral function at $0.62T_c$ for all quark masses. For the lightest quark studied by us ($\kappa=0.1325$), some system modification is already seen at $1.24T_c$, and the modification becomes larger as one goes to $1.5T_c$. For the next heavier quark ($\kappa=0.13$), at $1.24T_c$ the correlators agree completely with the reconstructed correlators, and one sees temperature modification of the pseudoscalar only at the higher temperature. For our heaviest quark ($\kappa=0.1234$), Fig. 11(a) shows that the pseudoscalar correlator is completely explained by the spectral function up to at least $1.5T_c$. The vector channel shows a similar trend, with the lighter quarks showing larger medium modification at a given temperature. For the scalar and axial vector channels, we found significant medium modifications similar to Figs. 6(b) and 9(b) for all three quark masses, indicating that also for the heaviest quarkonia studied by us, the $1P$ states undergo significant medium modification, possibly dissolution, already at $1.24T_c$.

VI. DISCUSSION OF POSSIBLE SYSTEMATIC ERRORS IN MEM ANALYSIS

The extraction of the continuous spectral function from $O(10)$ data points is, to start with, a rather delicate problem,

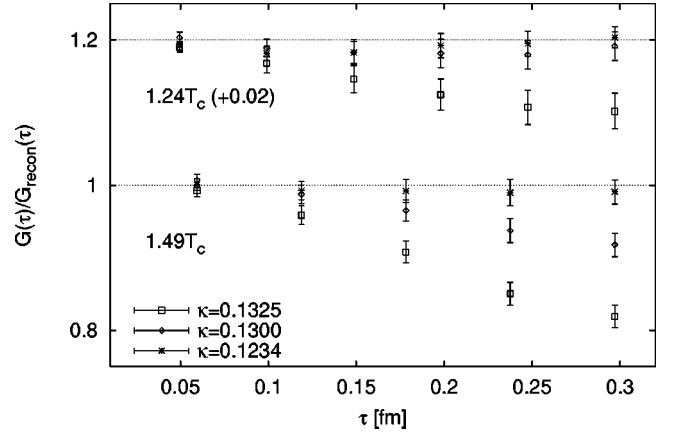


FIG. 11. The mass dependence of $G(\tau, T)/G_{\text{recon}}(\tau, T)$ at different temperatures, for the pseudoscalar channel. The reference spectral function used for $G_{\text{recon}}(\tau, T)$ is $\sigma(\omega, 0.62T_c)$. For clarity, the points at $1.24T_c$ have been shifted vertically, as indicated in the figure.

and one needs to understand the effect of the systematics well before drawing physics conclusions. In this section, we are going to discuss possible systematic effects in the spectral functions presented in Secs. IV B and V. One obvious problem is that at high temperature both the number of data points and the physical extent of the temporal direction become small, which makes the reconstruction of the spectral functions difficult [13]. To some degree this problem can be overcome if one uses the information about the high-energy behavior of the spectral function extracted at low temperatures, as was discussed in Sec. IV. This issue will be discussed here in more detail.

We start the discussion of the systematic effects for spectral functions corresponding to ground state, i.e., pseudoscalar and vector ones. In our method of analysis, the spectral function below T_c plays a crucial role since we extract the high-energy information from it, and we examine first the default model dependence of this spectral function. In Fig. 12 we compare the pseudoscalar and vector spectral functions at $0.75T_c$, reconstructed using the free massive lattice spectral function as a default model, with those shown in Sec. IV where the massless continuum spectral function was used as a default model. For the quark mass in the free lattice model, we use $ma \approx 0.17$, which corresponds to the bare mass for this set. As one can see from the figure, the dependence on the default model is quite small, even though the two default models have very different structures. For comparison, the masses extracted from the spatial correlators at this temperature are also shown as vertical lines. There is a small deviation between the peak position and the screening masses, $\sim 3\%$ for the pseudoscalar channel and $\sim 7\%$ for the vector channel. Since we do not expect medium modification of quarkonia properties below deconfinement (cf. Fig. 5), this should be interpreted as systematic error in our MEM analysis. Similar statements also hold for the spectral functions at $0.9T_c$.

Therefore, our way of using the information from the high ω part of the spectral function below T_c in the default model for the analysis above T_c removes the arbitrariness of the

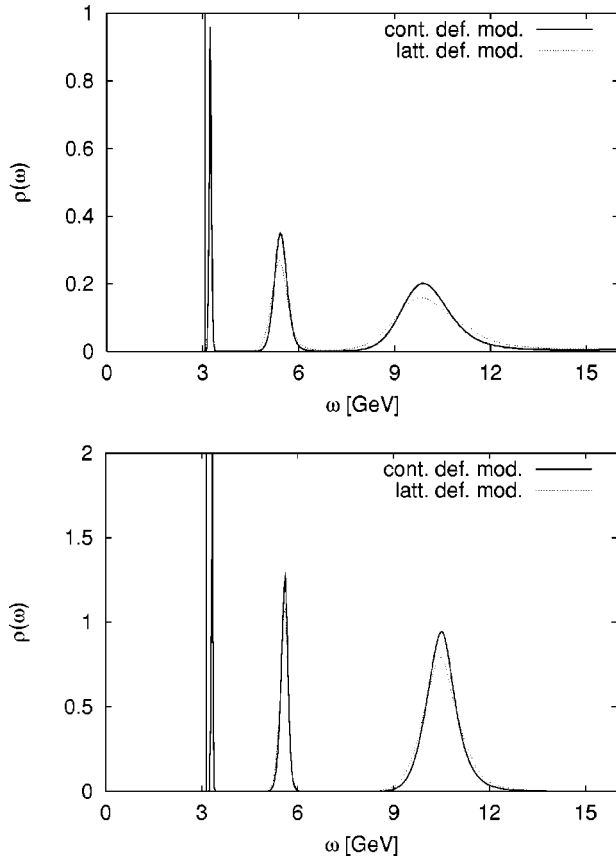


FIG. 12. The pseudoscalar (top) and vector (bottom) spectral functions at $0.75T_c$ reconstructed using the lattice and continuum default model (see text for further details).

default model. To check this, in Fig. 13 we redo the analysis presented in Fig. 10, where now the high ω part was taken from the spectral function at $0.9T_c$ calculated with the free massive lattice default model with the corresponding mass. For comparison, we also show the spectral function at $0.9T_c$ recalculated with this default model. As one can see, the main features of Figs. 13(a) and 13(b) are very similar to those of Figs. 10(a) and 10(b), respectively, so that one can essentially substitute them without having to change any of the discussion following Fig. 10.

Another question to be addressed is to what extent the temperature modification of the spectral functions seen in Sec. V and Fig. 13 is real physical effect, as opposed to the offshoot of the inability of the MEM to correctly reproduce the spectral function from the small number of data points and small temporal extent available at higher temperatures. To answer this question, we compare in Fig. 14 the spectral functions for set III at different temperatures constructed using the same number of data points. In the three panels of Fig. 14(a) the pseudoscalar spectral functions at different temperatures are constructed with the same number of data points as are available for the highest temperature in the panel, omitting points from the center for the lower temperatures. N_{data} here refers to the number of points after periodic folding. Though the figure shows that the details of reconstructed spectral functions depend on the number of data points used in the analysis, it is clear that the fact that sub-

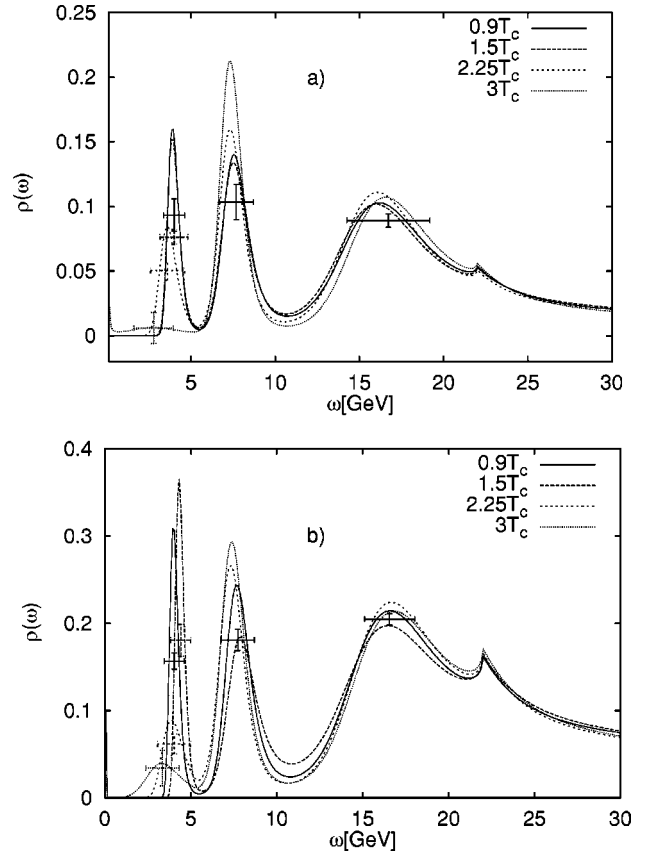


FIG. 13. The spectral functions for (a) pseudoscalar and (b) vector channels at different temperatures for set III, where the default model incorporates the high-energy part of the spectral function at $0.9T_c$ obtained using the free massive lattice spectral function (see text for further details).

stantial modification of the spectral function takes place at $2.25T_c$ and the ground state is “dissolved” at $3T_c$ is not an artifact of the limited resolution. Figure 14(a) also shows very clearly the absence of any significant change in the pseudoscalar channel up to $1.5T_c$. Similar comments also hold for the vector channel in Fig. 14(b). In this case, we do see the mass shift at $1.5T_c$ discussed before irrespective of N_{data} , but the exact amount of the shift differs.

In Fig. 15 we do a similar analysis for set II, where we reconstruct the spectral function at different temperatures using the same physical extent as available for $1.5T_c$. This figure shows that the seeming reduction of the peak strength at $1.5T_c$ in Fig. 8 was probably due to the small number of data points available there, and the pseudoscalar and vector peaks are not substantially changed up to $1.5T_c$, as one would expect from Fig. 6(a) and the results for set III.

Now let us discuss the scalar and axial vector channels. In Fig. 16 we show the spectral function in the scalar and axial vector channels at $0.9T_c$ and set III using the free massive lattice spectral function as a default model. Also shown there are the spectral functions for the free continuum default model from Sec. IV for comparison. As one can see, the spectral functions show a stronger default model dependence than the pseudoscalar and vector ones, though the main features of the spectral functions are independent of the default

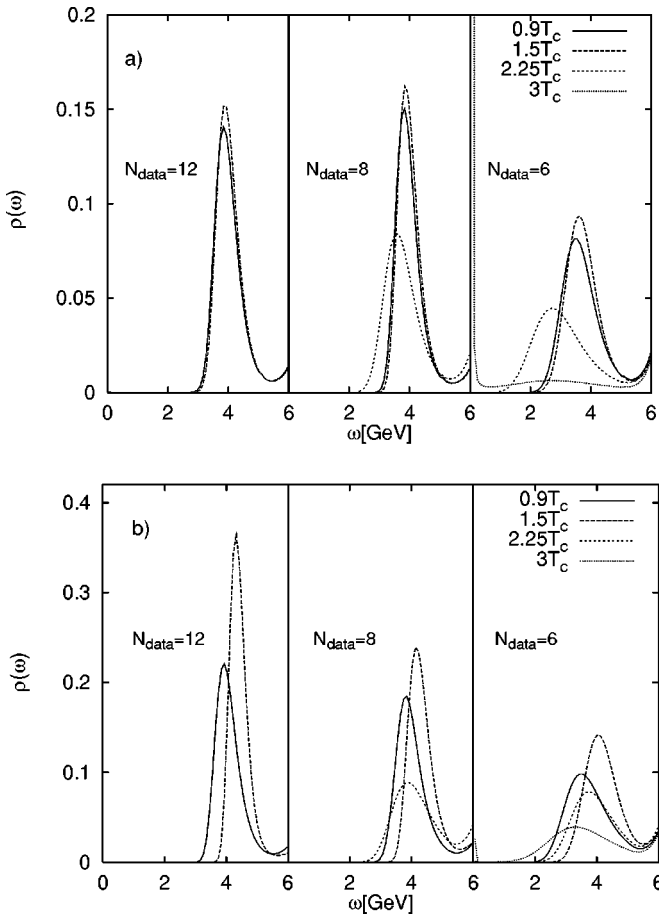


FIG. 14. The (a) pseudoscalar and (b) vector spectral functions at different temperatures reconstructed using the same number of data points at each temperature.

model. The stronger default model dependence is probably due to the fact that these correlators are noisier than the pseudoscalar and vector ones. The default model dependence of the scalar and axial vector spectral functions was found to be even stronger for set II at $0.75T_c$. If one uses the free massive lattice spectral functions as a default model at

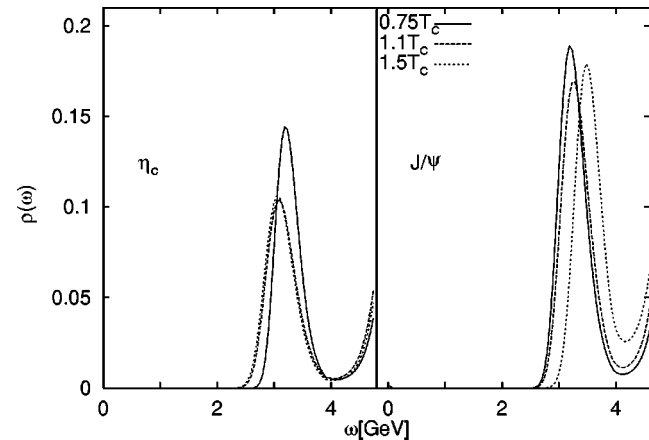


FIG. 15. Spectral functions for set II for pseudoscalar and vector with $N_{\text{data}}=6$ data points.

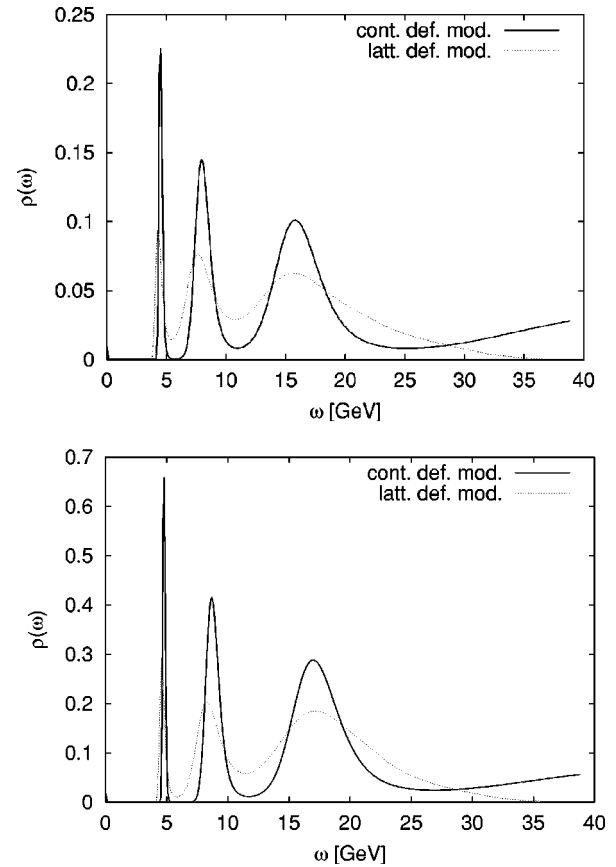


FIG. 16. Spectral functions for scalar (top) and axial vector (bottom) channels reconstructed using the continuum and the lattice free spectral function as a default model.

$0.75T_c$, a large reduction in the peak height of the χ_c state can be seen, though the position of the peak is roughly correct. This problem is also due to limited statistics. It turns out that the probability $P[\sigma|\alpha] = \exp(-\alpha S)$, which is expected to be strongly peaked around some α_{max} ideally (for large statistics), has a long tail at large α values in this particular case, so that the peak structure seen around α_{max} is smoothed considerably when one averages over α .

Finally, we also want to address the issue of whether the serious system modification, possibly dissolution, of the χ_c states at $1.12T_c$ seen in Fig. 7 is an artifact of the smaller number of data points at this temperature. In Fig. 17 we show the spectral functions in scalar and axial vector channels at $0.75T_c$ and $1.12T_c$ using $N_{\text{data}}=8$ data points and the same temporal extent. The figure clearly shows that the large change in the spectral function between $0.75T_c$ and $1.12T_c$ is a physical effect and not due to the small number of data points at the higher temperature.

So far all data above T_c have been analyzed using the high-energy part of the corresponding spectral functions below T_c . For set III at $1.5T_c$ we still have $N_{\text{data}}=12$ data points and not too small temporal extent. Therefore, here we can also reliably reconstruct the spectral function without providing precise information for the high ω region. Figure 18 shows the spectral function for J/ψ , reconstructed using both the free massless continuum and the free massive lattice

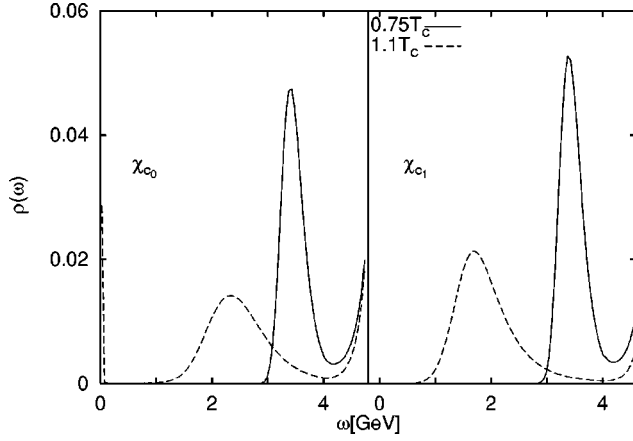


FIG. 17. Spectral functions from set II for scalar and axial vector with $N_{\text{data}} = 8$ data points at different temperatures.

spectral functions as the default model. Although some dependence on the default model is clearly seen, the strong ground-state peak is pretty stable and provides further evidence that the J/ψ survives well into the deconfined gluon plasma.

VII. SPATIAL CORRELATORS AND SCREENING MASSES

Most of the early studies of the finite-temperature meson spectrum concentrated on studies of correlators in one of the spatial directions (for convenience, we will use the z direction in what follows). The corresponding masses are usually referred to as the screening masses [34]. The spatial correlators are related to the same spectral function, but the relationship is a bit more complicated: the momentum-projected correlators in the z direction are given by [35]

$$G(i\omega_n, \vec{p}_T, z) = \int_{-\infty}^{\infty} \frac{dp_z}{2\pi} e^{ip_z z} \int_0^{\infty} dp_0 \frac{2p_0 \sigma(p_0, \vec{p}_T, p_z)}{p_0^2 + \omega_n^2}, \quad (24)$$

where \vec{p}_T is the transverse momentum in the xy plane and ω_n is the Matsubara frequency. The screening mass is obtained

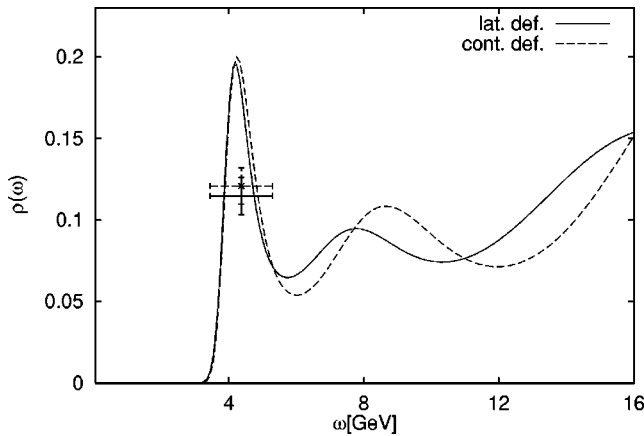


FIG. 18. The vector spectral function at $1.5T_c$ and set III using the free continuum and lattice spectral function as a default model.

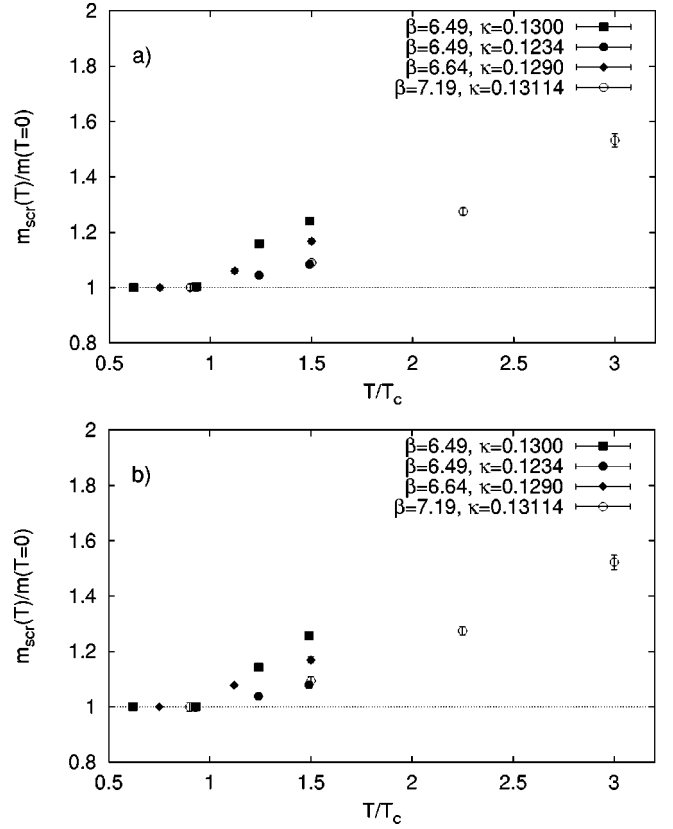


FIG. 19. Screening masses for the (a) vector and (b) pseudoscalar channels for the different sets, normalized by the zero-temperature mass (see text).

from the correlators projected to zero transverse momentum and zero Matsubara frequency.

While the screening masses, in general, are not directly related to the spectrum of the finite-temperature system, it is possible to extract important information from them, in particular for examining particular model spectral functions. In the presence of a stable bound state, which gives a contribution $\sim \delta(p_0^2 - \vec{p}^2 - m^2)$ to the spectral function, it can be easily seen from Eq. (24) that the screening mass is identical to the pole mass of the state.

Numerically, the study of screening masses is much simpler because of the large extent available in the z direction, and one can obtain the screening masses from standard one-exponential fits to the long-distance part of the correlator. Figure 19 summarizes the temperature dependence of the vector and pseudoscalar screening masses for the different sets studied by us. We have calculated them from one-exponential and two-exponential fits, and in all cases the two agree. In order to show the relative changes in screening mass with temperature, we have normalized the masses with the zero-temperature masses from Table IV, which, as mentioned in Sec. III, were obtained from the screening masses from the lowest temperature available to us for each set. So the part below T_c in Fig. 19 is just the normalization except in set I. From the figure, one makes the following observations.

(i) The screening mass does not change up to T_c (or at least until $0.93T_c$) for either channel. This observation is in agreement with what is seen for light quarks and glueballs. We also see that the screening masses below T_c are in agreement with the pole mass extracted from the temporal masses, wherever such an extraction is possible reliably.

(ii) The screening masses show a definite temperature effect above T_c , increasing steadily with temperature for both the channels. This effect is in sharp contrast to the temporal correlators, which indicated little temperature effect up to $\approx 1.5T_c$, in particular for the pseudoscalar channel. Since for the pseudoscalar channel, we do not see any shift in the ground-state peak position certainly up to $1.5T_c$, and possibly up to $2.25T_c$, Fig. 19(b) indicates that the pole and screening masses differ from each other, even though a bound state is present in the spectral function. For the vector case also, even though a small shift in the pole position may be present at $1.5T_c$, the shift of screening mass in Fig. 19(a) is much larger and indicates a similar difference between the pole and screening masses. One possibility that one has to consider is that while there is a bound state in the spectral function above T_c , it is not a δ -function state. We investigated the possibility of the screening mass change being caused by the state gaining a width above T_c , by using a Breit-Wigner form as found in Ref. [13], but our conclusion is that the change in screening mass is too large to be explained this way.

Another possible way that a screening mass can change differently from the pole mass, even in the presence of a bound state, is if the dispersion relation changes in the thermal medium [36,28]. Since in a thermal medium the Lorentz symmetry is lost, in general one would expect an energy-momentum asymmetric self-energy term, leading to a dispersion relation

$$\omega^2(\vec{p}, T) = m(T)^2 + \vec{p}^2 + \Pi(\vec{p}, T). \quad (25)$$

This will, in general, alter the screening mass from the pole mass. For small momenta, one can make the simplifying assumption that the modified dispersion relation can be approximated by a temperature-dependent mass and a temperature-dependent “speed of light” [36,28]

$$\omega^2(\vec{p}, T) = m^2(T) + A^2(T)\vec{p}^2. \quad (26)$$

For a δ -function state in the dispersion relation, Eq. (26) gives

$$m_{\text{scr}}(T) = m_{\text{pole}}(T)/A(T). \quad (27)$$

Such a modified dispersion relation can explain the discrepancy between the pole and screening mass if, for example, $A(T) < 1$ at $1.5T_c$.

This scenario can be checked by constructing the spectral function from the temporal correlators for nonzero momenta. Equation (26) with $A(T) < 1$ will lead to a less-than-relativistic shift in the spectral function peak with spatial momenta. Figure 20(a) shows the ground-state peak for the vector channel below and above T_c for set III, and Fig. 20(b) shows the same for the pseudoscalar channel. The vertical

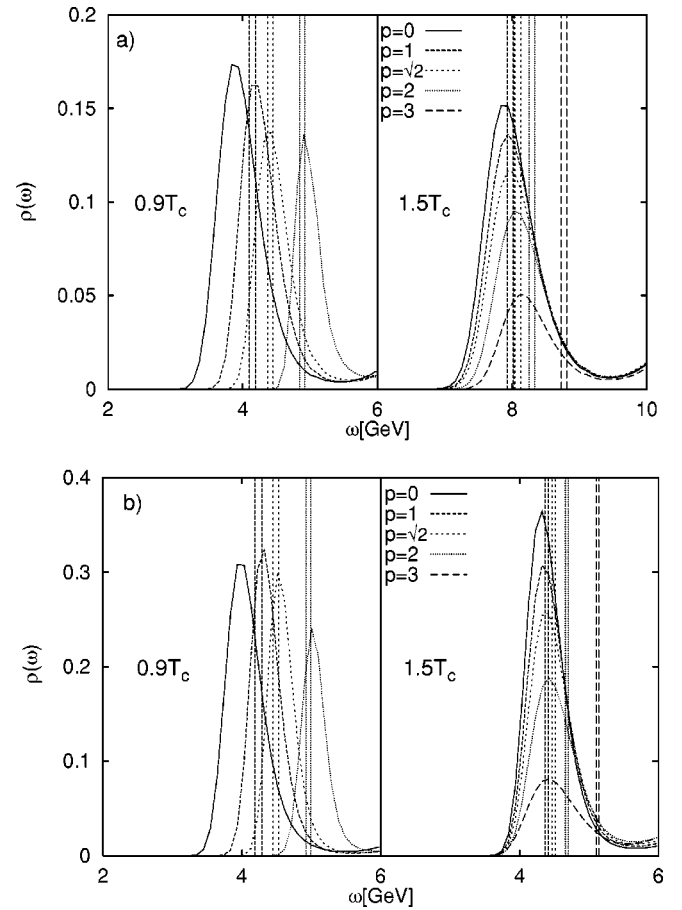


FIG. 20. Spectral functions for the (a) pseudoscalar and (b) vector channel for a few nonzero momenta, below and above T_c . The momenta are given in units of $2\pi/La$, where La is the transverse dimension of the lattice. The vertical bands show the expected peak positions for the nonzero momenta, assuming a relativistic dispersion relation.

bands in both figures show the expected peak positions for the nonzero momenta, assuming a relativistic shift from the peak at zero momentum. This was obtained by using the lattice form of Eq. (26) with $A(T) = 1$,

$$\cosh \omega(\vec{p}) - 1 = \sum_{i=1,2} (1 - \cos p_i) + \frac{m^2}{2}, \quad (28)$$

where all the variables ω , p_i , and m are in units of inverse lattice spacing. The width of the band reflects the uncertainty in the zero-momentum peak position due to the finite bin size. The shift of the peak position at $0.9T_c$ is seen to be consistent with the expected relativistic shift in both channels, in agreement with previous results that the Lorentz symmetry is approximately valid up to close to T_c [32,37]. At $1.5T_c$, one clearly sees a much smaller shift in the peak position, confirming the medium modification of the dispersion relation discussed above. A more quantitative analysis, to check whether the shift in the screening mass is completely due to such a modification of the dispersion relation,

cannot, however, be conclusively made due to the rather large uncertainty in determining the peak position from a maximum entropy analysis.

VIII. SUMMARY AND DISCUSSION

In this work, we have conducted a detailed lattice study of the properties of the $1S$ (η_c and J/ψ) and $1P$ (χ_c^0 and χ_c^1) charmonia in hot gluonic medium by studying the thermal correlators in Euclidean time and extracting spectral functions from them. We show that one can extract useful information about medium modifications of charmonia above T_c by comparing the correlators with those reconstructed from the spectral function below T_c . We also show that by providing correct information about the structure of the high-energy part of the spectral function, one can reliably extract the low-energy part of the spectral function at high temperatures from correlators measured at a limited number of points.

In the hadronic phase, we find that the properties of all the states remain unchanged at least up to temperatures of $0.93T_c$ as one approaches the deconfinement transition temperature from below. This is similar to quenched studies of light mesons and glueballs, and may not be true for full QCD.

As the temperature of the medium crosses T_c , significant modifications of the χ states are observed. The temporal correlators show large enhancement, and already at $1.1T_c$ the ground-state peaks are not observed in the spectral function, indicating that these states may have dissociated already at this temperature. The $1S$ states behave quite differently. Little change is seen in the correlators as one crosses T_c , and the spectral function shows a significant ground-state peak until quite high temperatures. No significant reduction of either the peak strength or the mass of the state is seen at least up to $1.5T_c$. At higher temperatures, the peak weakens, though at $2.25T_c$ one still finds a significant peak. (The apparent contradiction of this result with Ref. [14] has been discussed in Sec. V.) Finally, at $3T_c$ we do not observe any significant peak anymore, indicating that the state has broadened and weakened so much that it is not meaningful to treat it as a resonance any more.

These results have direct phenomenological implications, as $\rho(\omega)$ for the vector current is connected to the dilepton rate. Let us consider a hypothetical heavy-ion collision experiment which forms equilibrated gluon plasma, and whose temperature can be increased gradually. As one crosses T_c , one expects to see a reduction in the J/ψ peak in the dilepton channel caused by the disappearance of the excited states.

(We would like to remind the reader here that about 40% of all J/ψ produced in hadron collisions are indirect and come from χ_c and ψ' states.) The remaining J/ψ peak then stays stable as one increases the temperature further, showing little further reduction at least up to $1.5T_c$. On further increasing the temperature, the peak starts to “melt” gradually by weakening and possibly broadening. At $2.25T_c$ we see $\sim 25\%$ further reduction in the integrated strength of the J/ψ peak (for our quark mass). This process continues as one increases the temperature further, and by $3T_c$ the J/ψ peak is indistinguishable from the background.

It is reasonable to expect that the qualitative picture remains the same as one introduces dynamical quarks. Below T_c , there may be changes in the meson properties due to the activation of the thermal pions, and it is possible that the χ states dissociate even before T_c . For J/ψ itself, such thermal pions will have little effect, and above T_c , the gradual melting picture described above is likely to be still true qualitatively, with the thermal quarks causing only small quantitative changes.

These results are quite different from the earlier potential model studies, which predicted the $1S$ charmonia to be dissolved at $\sim 1.1T_c$ [2,3]. Since the appearance of our earlier studies [12], some of the potential model studies have been reanalyzed. It was pointed out in Ref. [38] that Ref. [2] does not take into account a possible rise in the strong-coupling constant near T_c , which will lead to a bound J/ψ deep in the plasma. Also a very thorough and detailed study of the color singlet potential conducted in Ref. [39] shows that the color singlet free energy and potential above T_c (up to a few times T_c) behave very differently from what was anticipated in Ref. [3] on perturbative grounds [40], and will probably give rise to a considerably higher dissolution temperature for the J/ψ . Be that as it may, it is not clear that a potential model study can capture all the physics going into the medium modification of J/ψ like the collision broadening due to thermal gluons. It will certainly be interesting to have an analysis based on potential models or other similar studies that can reproduce all the features of the direct studies by us (and others), which also rules out any substantial reduction of the mass of the J/ψ and η_c above T_c from its zero-temperature mass.

ACKNOWLEDGMENTS

We would like to thank Edwin Laermann and Sven Stickan for discussions. This research was funded by GSI under Contract BI-KAR, and by DOE under Contract No. DE-AC02-98CH10886.

-
- [1] T. Matsui and H. Satz, *Phys. Lett. B* **178**, 416 (1986).
 [2] F. Karsch *et al.*, *Z. Phys. C* **37**, 617 (1988).
 [3] S. Digal *et al.*, *Phys. Rev. D* **64**, 094015 (2001).
 [4] Y. Nakahara *et al.*, *Phys. Rev. D* **60**, 091503 (1999).
 [5] M. Asakawa *et al.*, *Prog. Part. Nucl. Phys.* **46**, 459 (2001).
 [6] QCD TARO Collaboration, Ph. de Forcrand *et al.*, *Phys. Rev.*

- D* **63**, 054501 (2001). See also Ref. [36] for an early attempt to extract pole mass from finite temperature temporal correlators.
 [7] F. Karsch and I. Wetzorke, in *Proceedings of Strong and Electroweak Matter 2000* (World Scientific, Singapore, 2001), p. 193.
 [8] CP-PACS Collaboration, T. Yamazaki *et al.*, *Phys. Rev. D* **65**,

- 014501 (2002).
- [9] I. Wetzorke *et al.*, Nucl. Phys. B (Proc. Suppl.) **106**, 510 (2001); P. Petreczky *et al.*, *ibid.* **106**, 513 (2001).
- [10] F. Karsch *et al.*, Phys. Lett. B **530**, 147 (2002); Nucl. Phys. **A715**, 701c (2003).
- [11] M. Asakawa, T. Hatsuda, and Y. Nakahara, Nucl. Phys. **A715**, 863 (2003).
- [12] S. Datta *et al.*, Nucl. Phys. B (Proc. Suppl.) **119**, 487 (2003).
- [13] T. Umeda *et al.*, hep-lat/0211003.
- [14] M. Asakawa and T. Hatsuda, Phys. Rev. Lett. **92**, 012001 (2004).
- [15] P. Petreczky *et al.*, hep-lat/0309012; P. Petreczky, hep-lat/0310059. See also Ref. [35].
- [16] M. Le Bellac, *Thermal Field Theory* (Cambridge University Press, Cambridge, England, 1996).
- [17] T. Hatsuda and T. Kunihiro, Phys. Rev. Lett. **55**, 158 (1985); Phys. Rep. **247**, 221 (1994).
- [18] E. Braaten, R. Pisarski, and T. Yuan, Phys. Rev. Lett. **64**, 2242 (1990).
- [19] F. Karsch *et al.*, Phys. Rev. D **68**, 014504 (2003).
- [20] B. Sheikholeslami and R. Wohlert, Nucl. Phys. **B259**, 572 (1985).
- [21] ALPHA Collaboration, M. Lüscher *et al.*, Nucl. Phys. **B469**, 419 (1996).
- [22] A. El-Khadra *et al.*, Phys. Rev. D **55**, 3933 (1997).
- [23] For example, for the pseudoscalar mesons we get 1.00 ± 0.03 (set IA), 0.96 ± 0.06 (IB), 0.91 ± 0.06 (IC), 0.95 ± 0.04 (II), and 1.02 ± 0.06 (III) for $M_{\text{pole}}/M_{\text{kin}}$, using Eq. (13). For the heavy-light pseudoscalars, it has been reported that a relation like $M_{\text{kin}} = M_{\text{pole}} + m_{\text{kinetic}} - m_{\text{pole}}$ works quite well for the meson masses; see, for example, UKQCD Collaboration, K. Bowler *et al.*, Nucl. Phys. **B619**, 507 (2001). For our heavy-heavy mesons, while consistent within errors, such a relation seems to underestimate the difference between kinetic and pole mass of the meson.
- [24] G.P. Lepage and P. Mackenzie, Phys. Rev. D **48**, 2250 (1993).
- [25] M. Göckeler *et al.*, Nucl. Phys. B (Proc. Suppl.) **53**, 896 (1997); Nucl. Phys. **B472**, 309 (1996).
- [26] S. Sint and M. Lüscher, Nucl. Phys. B (Proc. Suppl.) **63**, 856 (1998).
- [27] QCD TARO Collaboration, S. Choe *et al.*, J. High Energy Phys. **08**, 022 (2003).
- [28] E. Laermann and P. Schmidt, Eur. Phys. J. C **20**, 541 (2001).
- [29] M. Jarrel and J.E. Gubernatis, Phys. Rep. **269**, 133 (1996).
- [30] R.K. Bryan, Eur. Biophys. J. **18**, 165 (1990).
- [31] F. Karsch *et al.*, Phys. Lett. B **497**, 249 (2001).
- [32] N. Ishii *et al.*, Phys. Rev. D **66**, 014507 (2002); S. Datta and S. Gupta, *ibid.* **67**, 054503 (2003).
- [33] C. Michael and A. McKerrell, Phys. Rev. D **51**, 3745 (1995).
- [34] C. DeTar, Phys. Rev. D **37**, 2328 (1988).
- [35] F. Karsch and E. Laermann, in *Quark-Gluon Plasma*, edited by R.C. Hwa (World Scientific, Singapore, 2003), Vol. 3.
- [36] T. Hashimoto, T. Nakamura, and I.O. Stamatescu, Nucl. Phys. **B400**, 267 (1993).
- [37] B. Grossman *et al.*, Nucl. Phys. **B417**, 289 (1994); S. Datta and S. Gupta, *ibid.* **B534**, 392 (1998).
- [38] E. Shuryak and I. Zahed, hep-ph/0307267.
- [39] O. Kaczmarek *et al.*, hep-lat/0309121; Phys. Lett. B **453**, 41 (2002).
- [40] S. Nadkarni, Phys. Rev. D **34**, 3904 (1986).